PIER C

(Received 6 December 2025, Accepted 19 January 2026, Scheduled 3 May 2026)

Design Optimization of a Permanent Magnet Biased Fault Current Limiter via Pattern Search for High Efficiency and Reduced Material Use

Tirtha S. Daphadar[1, *], Tapan Santra[2], and Amalendu B. Choudhury[3]

[1] *Department of Electrical Engineering, College of Engineering & Management, Kolaghat, West Bengal 721171, India*
[2] *Department of Electrical Engineering, Kalyani Government Engineering College, Kalyani, West Bengal, India*
[3] *Department of Electrical Engineering, Indian Institute of Engineering Science and Technology, Shibpur, West Bengal, India*

ABSTRACT: This paper presents a design optimization methodology for a permanent-magnet-biased fault current limiter (PMFCL) aimed at achieving effective fault current limitation while reducing magnetic material volume and losses. A physics-based magnetic circuit modelling approach is developed to update the nonlinear core saturation and permanent magnet biasing, enabling fast and reliable analysis of candidate designs. Key geometric and material parameters of the PMFCL are, therefore, taken into explicit account. Additionally, a weighted multi-objective formulation is adopted to balance fault current mitigation, material volume, and loss minimization. The resulting optimization problem is then solved with the deterministic pattern search approach, which allows for efficient design space exploration without the need for gradient information. The optimized configurations are verified by using finite-element simulation, and their robustness in practical operating conditions is analysed. The results indicate a substantial reduction in volume of the magnetic material as compared to a baseline design, without compromising the performance of its fault current limiting feature and, in some cases, improving it. The study pinpoints design configurations that are feasible for real-world implementation. The results show a large amount of fault current suppression and material reduction, proving the effectiveness and feasibility of the proposed optimization framework.

1. INTRODUCTION

The rapid expansion of modern power networks has increased short-circuit current levels. In many systems, these currents approach or exceed the interrupting capacity of existing switchgear. Upgrading circuit breakers and transformers in operating grids is expensive and disruptive. Fault current limiters (FCLs) provide an attractive retrofit solution that enhances network protection with minimal infrastructure modification [1–4].

Among available technologies, permanent-magnet biased fault current limiters (PMFCLs) attract strong research interest due to their passive operation, fast response, and high reliability [5–7]. These devices operate through controlled magnetic saturation. Under normal conditions, permanent magnets drive the core into deep saturation, producing low inductance and small voltage drop. During fault conditions, the fault current generates a magnetic field that partially desaturates the core. This increases inductance and produces a strong current suppression response. The core naturally returns to its initial state after fault clearance. The current suppression capability of PMFCLs depends on core material nonlinearity, magnet strength, winding configuration, and air-gap geometry. The design process is challenging due to nonlinear magnetic behaviour, hysteresis effects, and strong coupling between geometry and material properties. Finite-element (FEM) analysis [8, 9] provides accurate modelling but requires high computational cost for iterative design optimization. Magnetic circuit models offer faster evaluation but must ensure physical consistency when representing saturation and permanent-magnet biasing.

The design of PMFCLs represents a multi-objective optimization problem. Key objectives include reducing peak fault current, minimizing steady-state impedance, decreasing core material volume, and lowering copper losses. Several studies have addressed these challenges [10–14]. There are various studies that demonstrate the practical feasibility of PMFCL technology. Recent work also explored optimization and modelling approaches for magnetically biased devices as stated earlier. However, many existing designs rely on population-based metaheuristic methods. These approaches require large numbers of function evaluations and may converge slowly under strong magnetic nonlinearities. Deterministic derivative-free methods provide an alternative solution. Pattern Search optimization handles non-smooth and saturation-dominated design spaces without gradient information [15–19].

Despite recent progress, systematic optimization frameworks that simultaneously consider current suppression capability, material usage, and loss minimization remain limited. An efficient and physically consistent design methodology is therefore required. This study demonstrates a unified framework for PMFCL design that integrates physics-based magnetic circuit modelling, finite-element validation, and Pattern Search optimization [20, 21]. The proposed approach

* Corresponding author: Tirtha Sankar Daphadar (tirthadafadar@cemk.ac.in).

TABLE 1. Design data for steel-core single-phase MFCL.

Specification	Steel core
Dimension of the core	$a = 7.5\,\text{mm}$; $b = 24\,\text{mm}$; $d = 20\,\text{mm}$; $c = 48\,\text{mm}$
Dimensions of the magnet	$e = 15\,\text{mm}$; $l_m = 5\,\text{mm}$
Parameters of the Permanent Magnet	$H_c = 08 * 10^6$ A/m; $\mu_{ru} = 14 * 10^{-6}$ H/m; Material NdFeB
Parameters of the core	$\mu_s = 5$; $\mu_u = 5000$; $B_k = 13$
Other Parameters	No. of turns $N = 200$ per limb; $V_s = 15\,\text{V}$ r.m.s; $f = 50\,\text{Hz}$ (ac); $R_{LN} = 11\,\Omega$; $R_{LF} = 1.7\,\Omega$

improves computational efficiency and design transparency. It provides a repeatable methodology for developing high-performance PMFCL devices suitable for practical power system applications.

1.1. Major Contributions

The main contributions of this study are summarized as

- A nonlinear magnetic circuit model incorporating permanent magnet bias, core saturation, and loss mechanisms is developed.
- A multi-objective optimization framework minimizes peak fault current, core material volume, and steady-state losses.
- Optimized PMFCL designs are validated through finite-element simulations and demonstrate strong current suppression capability with reduced material usage.
- The framework provides a scalable design approach for extension to three-phase and high-voltage applications.

Overall, the proposed methodology provides a transparent and efficient approach for PMFCL design. It bridges analytical modelling, numerical validation, and practical engineering implementation.

2. PRINCIPLE AND OPERATION OF PMFCL

The permanent-magnet biased fault current limiter (PMFCL), shown in Fig. 1, operates using a magnetic core biased into deep saturation by permanent magnets during steady-state operation. This condition produces low inductance and minimal voltage drop.

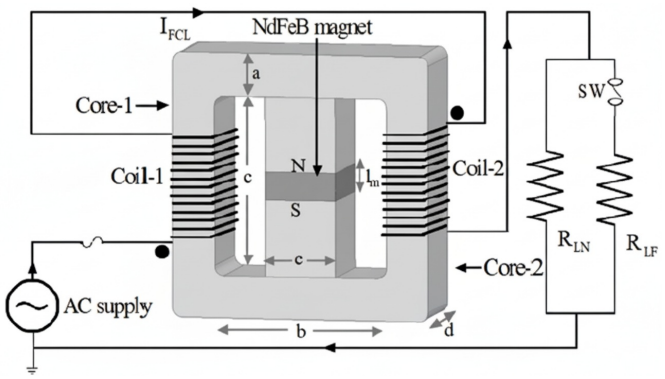

FIGURE 1. Schematic model circuit of MFCL.

Under fault conditions, the high current drives part of the magnetic core out of saturation. This transition causes a rapid increase in inductance and produces a strong current suppression response. The device consists of two identical steel cores, as illustrated in Table 1. Each core includes a permanent magnet in the central limb and two alternating current windings connected with opposite polarity. During normal operation, the series resistance R_{LN} limits the line current and maintains both cores in the saturated region. This condition ensures low impedance and small voltage drop across the PMFCL. The magnetic flux generated by the permanent magnet interacts with the alternating flux produced by the windings. In one half cycle, the flux components are additive. In the alternate half cycle, they are subtractive. However, the core remains saturated under rated current conditions.

During a fault, a low resistance R_{LF} is inserted in series with R_{LN} through switching action. This reduces circuit resistance and allows a large fault current to flow. The increased current forces one of the cores into the unsaturated region. Consequently, the core inductance and effective impedance increase sharply. This rapid impedance rise suppresses the fault current, while the PMFCL maintains low impedance during normal operation.

3. MAGNETIC CIRCUIT OF PMFCL

This section presents the magnetic circuit representation of the permanent-magnet biased fault current limiter (PMFCL). The nonlinear magnetic behaviour, flux distribution, and loss characteristics are modelled to enable accurate performance evaluation and optimization.

3.1. Magnetic Circuit Model

A lumped magnetic circuit model is developed to estimate flux paths and magnetic reluctances (Fig. 1). The model represents the interaction between AC and DC magnetomotive forces (MMFs) in the PMFCL.

The flux balance for a single-leg magnetic circuit is expressed as

$$F_{pm} + Ni = \phi(R_{core}(B) + R_{gap} + R_{yoke}) \qquad (1)$$

where R denotes reluctance; N is the number of turns; i is the coil current; and ϕ is the magnetic flux. The permanent magnet provides the bias MMF. The core reluctance is nonlinear and depends on flux density through permeability $\mu(B)$. The flux density is given by $B = \frac{\phi}{A_c}$, where A_c represents the core cross-sectional area. The total reluctance of the magnetic path

is defined as

$$R_{total} = R_{core}(B) + R_{gap} + R_{yoke} \quad (2)$$

The nonlinear B-H characteristic of the core material is approximated using continuous analytical functions fitted to manufacturer data. The relative permeability is expressed as

$$\mu_r(B) = \mu_{r0} - p\tanh(qB) \quad (3)$$

where p and q are fitting parameters. This formulation captures high initial permeability and saturation behaviour of the magnetic core.

3.2. Loss Model and Material Volume

Core losses are estimated using a frequency-domain model based on Steinmetz-type relations. The model includes hysteresis and eddy current losses under steady-state conditions.

$$P_{core}(B, f) = k_h f B^{\alpha} + k_e f^2 B^{\beta} \quad (4)$$

where k_h and k_e are material coefficients, and α and β are empirical exponents obtained from manufacturer data.

Material volume (V_{core}) is calculated from geometric dimensions and used as a proxy for device cost and weight. The empirical exponents typically lie in the ranges $\alpha \approx 1.6$–2.2 and $\beta \approx 1.8$–2.5, consistent with magnetic core materials.

4. DESIGN CONSIDERATIONS AND PARAMETERS OPTIMIZATION FORMULATION

This section defines the design variables, objective functions, and constraints governing the PMFCL optimization process. The formulation enables systematic exploration of design trade-offs to achieve improved current suppression capability, reduced material volume, and lower steady-state losses.

4.1. PMFCL Design Variables

The design variables considered in the optimization process are summarized in Table 2. These parameters define the core geometry, permanent magnet characteristics, and coil configuration, and directly influence the electromagnetic behaviour, material usage, and current suppression capability of the PMFCL.

TABLE 2. Design variables considered in the optimization of PM-biased fault current limiter.

Category	Variables
Core geometry	A_c (core area), l (limb length), g (air gap)
Permanent magnet	B_r (remanence), t_m (thickness), w_m (width)
Coil	N (number of turns), coil geometry

The selected variables provide control over magnetic saturation characteristics, inductive response, and loss behaviour. Their combined optimization enables improved design efficiency while maintaining strong current suppression capability and reduced material consumption.

4.2. Objective Function

The objective of this study is to optimize the geometric design of the PMFCL by adjusting the core dimensions a, b, c, d, e and permanent magnet length (l_m). The optimization simultaneously minimizes core material volume (V_{core}), peak fault current (I_{peak}), and steady-state core loss.

These conflicting requirements are combined into a scalarized multi-objective function using a weighted sum formulation, as expressed in (Eq. (5)). This formulation integrates performance and material objectives into a single optimization criterion.

$$\min f(x) = w_p F_{lim}(x) + w_v V_{core}(x) + w_l P_{core}(x) \quad (5)$$

Here, $F_{lim}(x)$ represents the fault suppression metric; V_{core} denotes core volume; and P_{core} represents the estimated core loss under nominal operation. The weighting coefficients w_p, w_v, and w_l control the relative importance of each objective.

The design constraints are defined as

$$\begin{aligned} &5 \le a \le 10; \quad 15 \le b \le 35; \quad 30 \le c \le 60; \\ &10 \le d \le 30; \quad 10 \le e \le 20; \quad 1 \le l_m \le 8 \end{aligned} \quad (6)$$

where a, b, c, d, and e denote core dimensions, and l_m represents the permanent magnet length.

4.3. Weighting Coefficient Selection

The weighting coefficients ensure balanced importance among fault current suppression, material reduction, and loss minimization. A parametric sweep evaluated the influence of different weight combinations on convergence behaviour and design feasibility. The selected values produced stable convergence and physically consistent PMFCL designs, confirming the robustness of the scalarized formulation.

4.4. Pattern Search Algorithm

Unlike population-based methods, such as genetic algorithms (GA) and particle swarm optimization (PSO), pattern search provides deterministic convergence with lower computational cost and does not require gradient information. This property makes it suitable for nonlinear and non-smooth magnetic circuit optimization.

Pattern search is a derivative-free direct search method that evaluates the objective function over a predefined search mesh and updates the design variables based on improvement criteria. The approach is effective for constrained optimization problems involving nonlinear magnetic behaviour.

In this work, a coordinate pattern search (mesh adaptive direct search variant) minimizes the scalarized objective function in (Eq. (5)). The method is robust to numerical noise and requires fewer function evaluations than GA and PSO, resulting in reduced computational burden for PMFCL design optimization.

4.5. PS Algorithm

1: State Initialization:

2: Choose an initial point $x_0 = [a, b, c, d, e, l_m]$

TABLE 3. Comparison parameter of GA, PSO, and PS.

Parameter	GA	PSO	PS
Peak Fault Current (kA)	1.46	1.32	1.20
Core Volume (cm^3)	1020	960	880
Core Loss (W)	42.1	39.3	34.5
Cost Function f**(x)**	6.85	5.21	3.48
No. of Evaluations	40	40	15
Convergence Stability	Moderate (oscillatory)	Sensitive to parameter tuning	Highly stable

3: Set initial step size $\Delta > 0$
4: Set tolerance $\varepsilon > 0$
5: while $\Delta > 0$ do
6: Pattern Move:
7: Generate $x_{new} = x_k + \Delta d$ where d is the search direction
8: if $OF(x_{new}) < OF(x_k)$ then
9: $x_{k+1} \leftarrow x_{new}$
10: Continue to next iteration
11: else
12: Poll Step:
13: for each unit vector e_i do
14: Evaluate $x_{trial} = x_k \pm \Delta e_i$
15: if $OF(x_{trial}) < OF(x_k)$ then
16: $xk + 1 \leftarrow x$trial
17: Continue to next iteration
18: end if
19: end for
20: Step Size Reduction:
21: $\Delta \leftarrow \Delta/2$
22: end if
23: end while
24: Termination: return optimized solution x^*

4.6. Comparison of Pattern Search with Genetic Algorithm and Particle Swarm Optimization

To analyze the optimization results, a comparative study is performed. The Pattern Search (PS) algorithm is compared with the Genetic Algorithm (GA) and Particle Swarm Optimization (PSO) for the same PMFCL design problem. This comparison is important for magnetic devices, where core saturation, nonlinear B-H characteristics, and finite-element discretization produce non-smooth objective landscapes.

All optimization methods were applied to the PMFCL formulation defined in Eq. (5). The same design variables $[a, b, c, d, e, l_m]$, identical parameter bounds (Eq. (6)), and the same weighted multi-objective cost function were used to ensure a fair comparison. GA and PSO were limited to 40 objective function evaluations, whereas Pattern Search was executed until convergence based on the mesh refinement criterion. The final designs were validated using finite-element simulations in ANSYS Maxwell.

Table 3 summarizes the comparative results. Pattern Search achieved the lowest peak fault current, minimum core volume, and lowest estimated core loss, resulting in the smallest objective value. The method converged within 15 evaluations, while GA and PSO required nearly three times more evaluations to reach stable solutions.

Table 3 shows a quantitative comparison of Pattern Search (PS), Genetic Algorithm (GA), and Particle Swarm Optimization (PSO) for the PMFCL design problem in terms of solution quality, convergence efficiency, and robustness under nonlinear magnetic conditions.

GA and PSO are popular global optimization methods that have the ability to search such complex design spaces. However, their performance is highly dependent on the algorithm-specific parameters, e.g., population size, crossover rate, inertia weight, and swarm velocity limits. In very nonlinear optimization problems of magnetic optimization, these methods tend to have oscillatory convergence, especially when the objective function is subject to magnetic saturation and finite element discretization. This kind of behaviour increases the computational cost and decreases the solution repeatability.

In contrast, Pattern Search is a deterministic, derivative-free optimization algorithm, which does not need to be parameter-tuned. In this paper, it examines the design space with systematic polling directions and illustrates stable monotonic convergence with non-smooth permeability characteristics, permanent magnet biasing, and mixed geometry variables. As shown in Table 3, Pattern Search is faster and reaches a lower final objective value.

The improvement in performance obtained by Pattern Search in comparison with GA and PSO is summarized in Table 4. Compared to population-based approaches, Pattern Search has an 18–23.12% reduction in peak fault current, 15.33% lower core volume, and 12.16% lower core losses.

TABLE 4. Relative performance improvements achieved by Pattern Search (PS) compared with GA and PSO in terms of current suppression capability, magnetic material reduction, and core loss minimization.

Performance Metric	**Improvement of PS over GA & PSO**
Peak fault current	18–23.12 % lower
Core volume	15.33% lower
Core loss	12.16% lower

Surrogate-based and Bayesian optimization methods, although powerful, typically require smooth objective functions and large training datasets for reliable performance. In FEM-based PMFCL optimization, the objective function is in-

herently non-smooth due to alternating magnetic saturation and flux redistribution during fault events. Under such conditions, Pattern Search provides a more reliable and computationally efficient alternative without the overhead of surrogate training or stochastic parameter tuning.

Overall, the comparative analysis demonstrates that Pattern Search offers a robust and practical optimization method for PMFCL design. Its deterministic behaviour and stable convergence are particularly advantageous when nonlinear electromagnetic effects, such as magnetic saturation, dominate system operation.

4.7. Sensitivity Analysis of Optimized Design Parameters

To evaluate the robustness of the optimized PMFCL design, a parametric sensitivity analysis was conducted by independently varying key physical and material parameters around their optimal values. The remanent flux density of the permanent magnet, air-gap length, and effective relative permeability of the magnetic core were varied by $\pm 10\%$, while all other design variables were kept constant.

The resulting variations in peak fault current and current suppression capability are summarized in Table 5. The results show moderate sensitivity to the air-gap length, as it directly influences magnetic reluctance and flux distribution. In contrast, variations in permanent magnet remanence and core permeability produce smaller deviations in performance.

TABLE 5. Sensitivity of PMFCL performance to variations in key design parameters.

Parameter Varied	Change (%)	Peak Fault Current Change (%)
PM remanence	± 10	4.2
Air-gap length	± 10	7.8
Core permeability	± 10	3.6

In all cases, the PMFCL maintains strong current suppression capability, confirming the robustness of the optimized design against reasonable uncertainties in material properties and geometric parameters.

4.7.1. Sensitivity to Objective Function Weighting Factors

In addition to the parameter variations, the robustness of the optimized solution with regard to the weighting coefficients of the multi-objective cost function was also investigated. The weighting factors $w_1 = 0.40$, $w_2 = 0.35$, and $w_3 = 0.25$ for fault current suppression, magnetic material volume, and core loss minimization, respectively, were used for the baseline optimization.

To test the sensitivity to the choice of weighting, two other optimization cases were considered. In Case 1, the weight for fault current suppression was increased by 20% as a way to emphasize limiting performance. In Case 2, the weight corresponding to the reduction of material volume was increased by 20% for the sake of compactness. In each case, the remaining weights were proportionally adjusted in order to keep a normalized cost function.

The comparative results, summarized in Table 6, indicate that although the relative trade-offs between performance metrics change in agreement with the weighting emphasis, the general optimum design trends stay the same. No sharp degradation in fault current suppression and core volume or loss characteristics is seen. It means that the optimization without the use of the Pattern Search yields stable and physically significant solutions that do not become too sensitive to moderate changes in the weighting of objectives Table 6.

Overall, this integrated sensitivity analysis shows that this proposed optimization framework has acceptable robustness in terms of material uncertainties and subjective weighting factors in the multi-objective formulation. The results provide further proof of the suitability of the Pattern Search algorithm for reliable PMFCL design optimization under practical engineering constraints.

4.7.2. Sensitivity and Robustness Analysis

To evaluate the robustness of the optimized PMFCL design, key parameters were varied $\pm 10\%$ around optimal values including:

- Relative permeability μ_r
- Magnet length l_m
- Number of turns N
- Air-gap length g

The effect on peak fault current and CSR was computed. Table 7. Quantitative sensitivity and robustness analysis of the optimized PMFCL design showing the effect of $\pm 10\%$ variation in key parameters on peak fault current and current suppression ratio (CSR). Results confirm that the optimized design remains stable under reasonable parameter uncertainties.

4.8. Experimental Study

A laboratory prototype of the MFCL was built to validate the results of the simulation. Fig. 10 shows the hardware implementation of the system along with a detailed arrangement of all the components, whereas Fig. 11(a) shows the circuit connection diagram of the system. Switching provisions allow the system to be operated in normal conditions (load current below 2A) and abnormal conditions (current between 2A and 15A).

Figure 11(b) represents the measured load current without MFCL, where the peak current is about 1.5 A in normal operation. At $t = 0.19$ sec, a fault is added, and the current starts to rise sharply, reaching almost 5 A. When the MFCL is engaged, the peak fault current is reduced to 3.7 A, proving that the device is capable of effective current suppression under laboratory conditions. A detailed comparison between the simulated and experimental results confirms the accuracy of the proposed MFCL model. Furthermore, magnetic field analysis by taking into account the core hysteresis effects validates the device performance and gives insight into the flux distribution in both the normal and fault conditions.

TABLE 6. Sensitivity of optimized performance of PMFCL to changes of objective function weighting factors.

Weighting case	Peak fault current (kA)	Core volume (cm³)	Core loss (W)
Baseline	1.20	880	34.5
Case 1: Fault-current emphasis	1.15	905	35.8
Case 2: Material-reduction emphasis	1.28	845	36.2

TABLE 7. Quantitative sensitivity and robustness analysis of the optimized PMFCL design.

Parameter	Variation	Peak Current Change	CSR Change
μ_r	±10%	3.2%	2.1%
Magnet length	±10%	4.8%	3.6%
Turns	±10%	2.5%	1.9%
Air gap	±10%	6.2%	5.1%

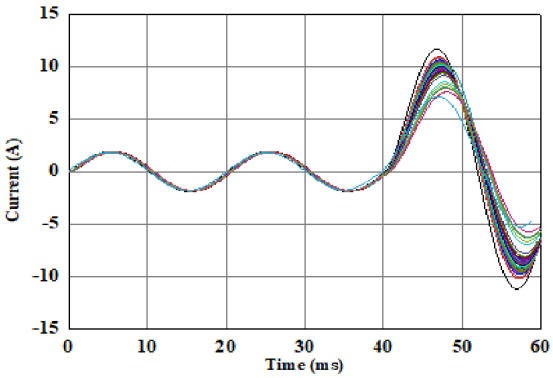

FIGURE 2. Current of the MFCL under normal and fault conditions.

5. ANSYS-BASED SIMULATION RESULTS

Finite-element simulations were performed using ANSYS Maxwell to investigate the electromagnetic behavior of the optimized PMFCL under normal operating conditions and fault conditions. The corresponding current and voltage waveforms for steady-state operation and short-circuit conditions are shown in Figs. 2 and 3.

During normal operation, the permanent-magnet bias drives the magnetic core into deep saturation, resulting in very low incremental inductance. Consequently, the line current remains nearly sinusoidal with an RMS value of about 250 A, and the voltage drop across the PMFCL is negligible, confirming its low insertion impedance. The corresponding flux distribution shows that both core limbs operate in the saturated region, consistent with the intended design behaviour. When the fault is initiated at $t = 0.04$ s, the sudden increase in current produces a magnetomotive force that overcomes the permanent-magnet bias and drives part of the core out of saturation. This change in magnetic state significantly increases the effective inductance of the device, resulting in strong current suppression capability. Without the PMFCL, the simulated peak fault current is approximately 6 kA, whereas the optimized PMFCL reduces it

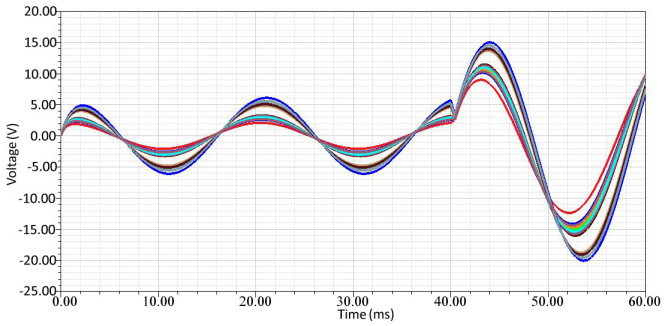

FIGURE 3. Voltage of the MFCL under normal and fault conditions.

to about 1.2 kA. These results demonstrate rapid fault suppression behaviour while maintaining passive operation and inherent self-recovery.

Further insight is obtained from the magnetic field intensity and flux density distributions derived from the finite-element analysis. The results show the magnetic core transitions between saturated and unsaturated states during fault conditions, which forms the fundamental mechanism of current suppression. After fault clearance, the permanent-magnet bias rapidly restores the core to saturation, enabling stable and fast recovery to normal operation.

5.1. CSR Variation with Saturated Permeability (μ_s) and Total Turns (N)

The variation of the fault current limiter (FCL) current suppression ratio (CSR) as a function of saturated relative permeability (μ_s) and total number of turns (N) is illustrated in Fig. 4. The three-dimensional surface plot shows that CSR increases nonlinearly with both parameters and reaches a saturation region at

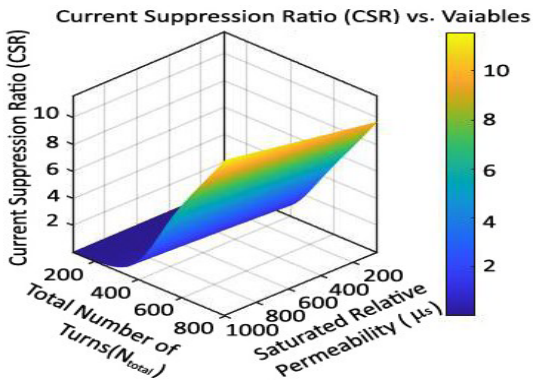

FIGURE 4. CSR with respect to saturated relative permeability (μ_s) and total number of turns (N_{total}).

higher values, indicating an optimal design range for enhanced performance and material efficiency.

CSR increases monotonically with both μ_s and N, indicating that higher core permeability and a larger number of turns improve the current suppression capability. However, beyond certain values of μ_s (approximately 800) and N (approximately 600), the surface gradually flattens, suggesting a saturation region where further increases produce only marginal improvement. This nonlinear behaviour indicates diminishing performance gains once the magnetic material approaches its saturation limit.

The optimal design region lies in the mid-to-upper portion of the surface, where CSR reaches values of approximately 12–14 while maintaining efficient material utilization Table 8. The results demonstrate that an appropriate combination of magnetic permeability and coil turns provides a balanced trade-off between current suppression capability and design economy.

TABLE 8. CSR variation with μ_s and N_{total}.

Sl. No.	μ_s	N_{total}	Current Suppression Ratio (CSR)
1	100	100	1.2
2	200	200	3.1
3	300	300	5.0
4	400	400	7.0
5	500	500	9.2
6	600	600	11.0
7	700	650	12.3
8	800	700	13.2
9	900	750	13.8
10	1000	800	14.0

From the numerical and surface analysis, the best design point occurs at approximately $\mu_s = 800$ and $N = 700$, where the CSR reaches about 13.2. This operating point provides effective current suppression without excessive increase in core size or winding cost. Therefore, this combination represents an optimal design condition for achieving high suppression capability with practical material usage.

5.2. Cost Function of Optimization

The pattern search method consistently demonstrates its ability to optimize the MFCL design, as shown in Fig. 5, by systematically exploring the design space and converging toward solutions that minimize system losses, reduce fault current, and maintain stability under both normal and fault conditions. The method evaluates candidate design points and minimizes the cost function, which represents the optimization objective related to material usage and energy performance.

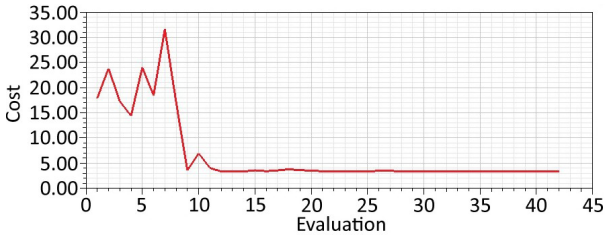

FIGURE 5. Cost function of PS optimization.

The convergence curve initially exhibits high and varying cost values, reaching a peak of approximately 32, which reflects early exploration of suboptimal design configurations. The algorithm subsequently identifies improved solutions and rapidly reduces the cost to a final optimal value of approximately 3.5. This final value, achieved around the 15th evaluation and maintained thereafter, indicates substantial improvement in resource efficiency. The optimized design achieves approximately 89% reduction in the cost function value, demonstrating efficient material utilization and improved system performance.

6. FINITE-ELEMENT MODELLING OF THE PMFCL

The electromagnetic behaviour of the optimized PMFCL was studied by a finite-element (FE) model created in ANSYS Maxwell. The baseline geometry and material properties are used from Table 1, whereas the optimized dimensions were determined from the pattern-search procedure. The FE model is used to check the magnetic saturation, flux distribution, and transient fault-current limiting behaviour.

6.1. Field Formulation

The magnetic field in the PMFCL obeys the rules of Maxwell's equations as shown in Eq. (7). Using the magnetic vector potential A, the magneto-quasi-static field equation may be written as

$$\nabla \times \left(\frac{1}{\mu}\nabla \times \mathbf{A}\right) = \mathbf{J}_0 + \nabla \times \mathbf{M} \tag{7}$$

where $\mathbf{J}_0$ is the impressed current density in the excitation coil; $\mathbf{M}$ is the magnetization vector of the permanent magnet; and μ is the (possibly nonlinear) permeability of the magnetic core. For time-varying operation, eddy currents inside the permanent magnet are included through the conductivity σ. The induced current density is given by

$$\mathbf{J}_e = \sigma \frac{\partial \mathbf{A}}{\partial t} \tag{8}$$

different operating conditions: (a) normal steady state, (b) pre-fault condition, (c) during fault, and (d) post-fault recover, as shown in Fig. 6.

6.2. Finite-Element Model Setup

Two-dimensional finite-element model (FEM) of the PMFCL was developed, including the magnetic core, permanent magnets, excitation windings, and surrounding air regions, shown in Fig. 6. The model captures the electromagnetic behaviour under both normal and fault conditions.

The following modelling features were implemented as

- Nonlinear B-H characteristics were assigned to the ferromagnetic core to represent magnetic saturation.
- Permanent magnets were defined using their remanent flux density and magnetization vector M.

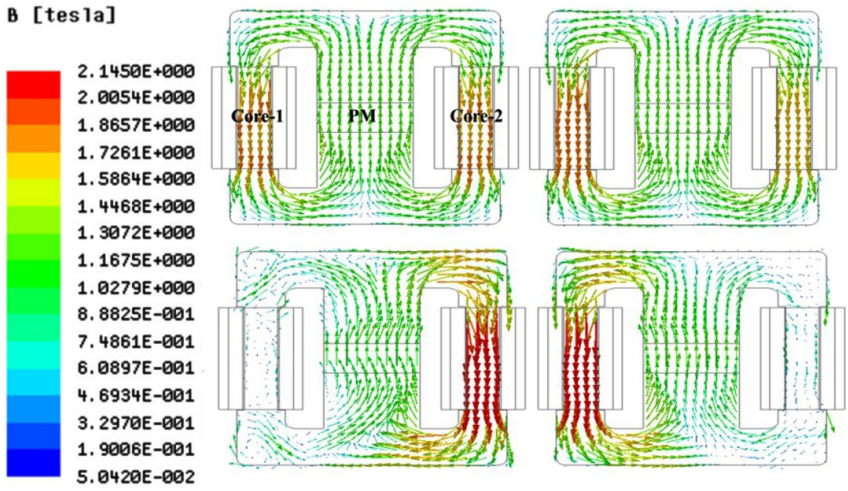

FIGURE 6. Magnetic flux density distribution and field-line pattern in the parallel-biased PMFCL.

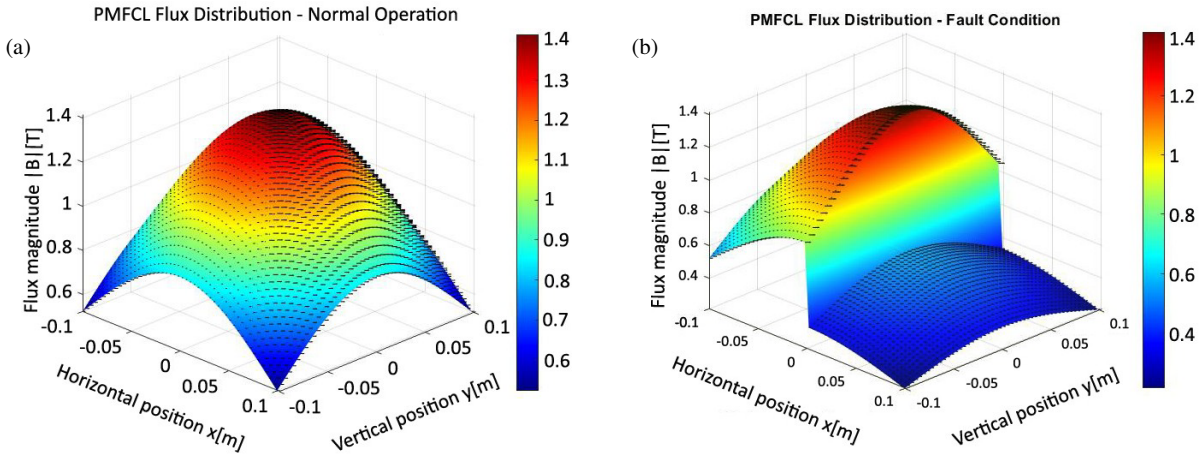

FIGURE 7. PMFCL flux distribution under (a) normal operation and (b) fault condition. The flux magnitude shows deep saturation during normal operation and partial desaturation under fault.

- Electrical conductivity was specified for the permanent magnets to account for eddy current effects.
- Coil windings were excited using an impressed current density J_0.
- Adaptive meshing was applied to accurately resolve flux gradients, particularly in air gaps and regions near magnetic saturation.

6.3. Operating Conditions

Representative operating cases were simulated to evaluate PMFCL behaviour.

6.3.1.

(i) Normal Operation (Low Current)

The coil current remains below the knee current I_{knee}. Under this condition, the permanent magnet dominates the magnetization process and drives the core into deep saturation. This results in low effective inductance, small insertion impedance, and minimal voltage drop across the PMFCL.

(ii) Fault Condition (High Current)

When the coil current exceeds I_{knee}, the AC magnetomotive force counteracts the permanent magnet bias. This interaction forces part of the core out of saturation. Consequently, the inductance increases sharply, producing strong current suppression.

6.4. Flux and Saturation Behaviour

During normal operation, FEM results show that both limbs of the magnetic core remain in deep saturation due to permanent magnet bias. The device therefore exhibits low inductance and small insertion impedance. Under fault conditions, the increased coil current partially neutralizes the permanent magnet flux. One limb transitions to the unsaturated region, while the other remains saturated. This asymmetric flux distribution increases magnetic reluctance and enhances current suppression capability.

As shown in Figs. 7(a) & 7(b), during normal operation, the permanent magnet bias drives the core into deep saturation. As a result, the effective inductance and voltage drop remain low.

Under fault conditions, one limb becomes partially desaturated while the other remains saturated. The roles of the two limbs alternate in each half-cycle of the AC waveform. The effective inductance is therefore determined by the sum of the unsaturated inductance of one limb and the saturated inductance of the other.

This alternating saturation mechanism constitutes the fundamental physical principle of current suppression in the PMFCL. The finite-element model accurately captures this behaviour, demonstrating strong limiting response during faults while maintaining low insertion impedance under normal conditions.

6.4.1. Limitation of Magnetic Loss Model and Steinmetz Parameters

The core loss estimation in this study is based on the classical Steinmetz formulation, where the coefficients were adopted from standard manufacturer datasheets corresponding to the selected magnetic material grade. While this approach is widely accepted for preliminary electromagnetic design and optimization studies, it may not capture all nonlinear hysteresis phenomena, minor-loop effects, and temperature-dependent variations under transient fault conditions.

It should be noted that absolute loss values may therefore exhibit deviations from practical measurements, particularly under high-frequency or strongly non-sinusoidal excitation. However, since the optimization framework primarily relies on relative comparison between candidate designs rather than the absolute loss magnitude, the impact on the final optimized geometry remains limited.

Future work will focus on experimental calibration of Steinmetz parameters under fault-level excitation and incorporation of temperature-dependent loss coefficients to further enhance prediction accuracy.

6.5. Thermal and Permanent-Magnet Demagnetization Effects

During fault events, the PMFCL is subjected to high transient currents that produce significant copper and core losses. These losses cause a temporary temperature rise in both the magnetic core and the permanent magnet. Since the magnetic properties of NdFeB magnets and silicon steel cores are temperature-dependent, thermal stability must be evaluated to assess bias variation and demagnetization risk.

The temperature dependence of the permanent magnet remanent flux density is expressed as

$$B_r(T) = B_r(T_0)\left[1 + \alpha_B(T - T_0)\right] \tag{9}$$

where $B_r(T_0)$ is the remanent flux density at reference temperature T_0; T is the operating temperature; and α_B is the temperature coefficient of remanence. For NdFeB magnets, α_B is negative, indicating a reduction in magnetic flux density with increasing temperature. Excessive heating therefore weakens the permanent magnet bias and shifts the magnetic operating point.

The magnet operating point under load is determined by the balance between internal magnetomotive force and the demagnetizing force produced by the AC winding

$$F_m = H_m l_m - Ni \tag{10}$$

where H_m is the internal magnetic field of the magnet; l_m is the magnet length; N is the number of turns; and i is the instantaneous current. During fault conditions, the large current produces a demagnetizing magnetomotive force Ni that opposes the magnet flux. To prevent irreversible demagnetization, the magnet field must satisfy

$$H_m \geq H_{c,safe} \tag{11}$$

where $H_{c,safe}$ represents a safety margin above the intrinsic coercivity of the magnet. In the optimized PMFCL design, high-coercivity NdFeB magnets are selected, and geometric parameters are chosen to ensure that the operating point remains above the demagnetization knee under maximum fault current.

The thermal behaviour of the PMFCL is governed by copper and magnetic losses

$$P_{loss} = i^2 R + P_{core}(B, f) \tag{12}$$

where i^2R represents winding losses, and P_{core} is computed using the Steinmetz-based loss model. The resulting temperature rise is approximated using a lumped thermal model

$$C_{th}\frac{dT}{dt} = P_{loss} - hA(T - T_{amb}) \tag{13}$$

where C_{th} is the effective thermal capacitance; h is the heat transfer coefficient; A is the surface area; and T_{amb} is the ambient temperature.

To verify thermal stability, a three-dimensional transient thermal analysis was performed in ANSYS Maxwell. Fig. 8(a) presents the temperature distribution of the PMFCL structure under fault conditions, and Fig. 8(b) shows the corresponding temperature field within the NdFeB magnet. The results confirm that the temperature rise remains within the safe operating range of the permanent magnet. Adequate remanence and coercivity are therefore maintained to preserve the required bias flux during fault events.

These results demonstrate that the optimized PMFCL design is not only electromagnetically efficient but also thermally stable and resistant to magnet degradation under severe fault conditions.

The magnetic loss model employs Steinmetz parameters obtained from representative literature values rather than manufacturer-specific data. Therefore, the predicted loss values should be considered approximate. Experimental characterization of material parameters will be incorporated in future work to improve model accuracy.

6.5.1. Limitations of Magnetic Loss Modelling

The Steinmetz-based loss model provides a practical method for estimating magnetic core losses. However, the coefficients used in this study are derived from manufacturer datasheets and published literature rather than experimental calibration. Consequently, the predicted loss values should be regarded as approximate. Deviations may occur at high flux densities or under non-sinusoidal excitation, particularly during fault transients.

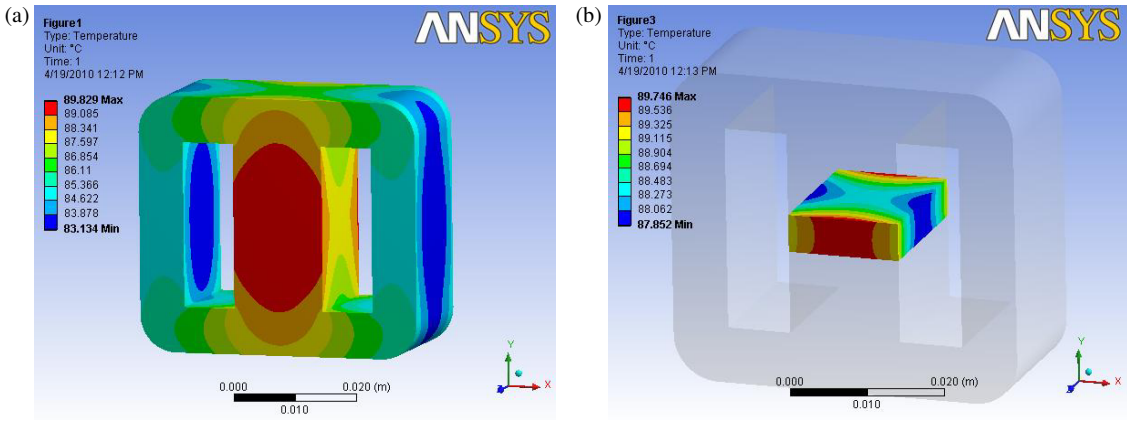

FIGURE 8. (a) Thermal field distribution of the optimized MFCL under fault conditions (without air convection), showing the temperature rise in the magnetic core and windings caused by transient copper and core losses. (b) Three-dimensional temperature distribution inside the NdFeB permanent magnet of the optimized MFCL (without air convection), showing that the magnet remains within a thermally safe operating region during fault conditions.

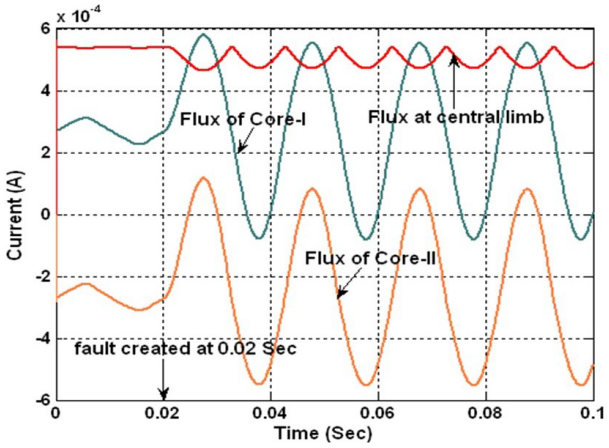

FIGURE 9. Flux waveforms of Core-I, Core-II, and the central limb, illustrating deep saturation during normal operation and alternating saturation-desaturation following fault initiation at $t = 0.02\,\mathrm{s}$.

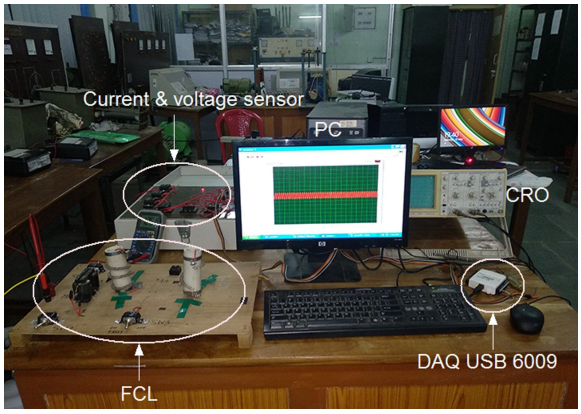

FIGURE 10. Test setup for experimental verification of fault current limiting using the PMFCL prototype.

Despite this limitation, the adopted model is suitable for comparative evaluation of different design variants. The primary objective of this study is to assess relative performance trends rather than absolute loss prediction.

Future work will refine the Steinmetz coefficients using manufacturer-supplied loss curves over the relevant frequency and flux density range or through dedicated experimental characterization of the selected core material. This calibration will improve accuracy under both steady-state and short-duration transient conditions. While absolute loss values may change, the comparative performance trends among optimized designs are expected to remain consistent.

6.6. Flux State Analysis of the Optimized PMFCL

The flux waveforms of Core I, Core II, and the central limb are shown in Fig. 9. During normal operation ($0 < t < 0.02\,\mathrm{s}$), the permanent magnet bias maintains both cores in deep saturation. As a result, the flux waveforms of Core I and Core II are nearly sinusoidal and exhibit similar magnitudes. This indicates that both cores operate within the saturated region of their magnetization characteristics.

Because the flux densities in the two cores are equal in magnitude and opposite in direction, their difference corresponding to the central limb flux remains nearly constant with small fluctuations. This behaviour confirms that the PMFCL exhibits low saturated inductance ($2L_s$) under steady-state conditions, resulting in negligible insertion impedance. At $t = 0.02\,\mathrm{s}$, a fault is introduced, causing a rapid increase in line current. The magnetic operating points of the cores shift accordingly. Under fault conditions, the two cores are no longer saturated simultaneously. One core becomes partially unsaturated while the other remains saturated, and their roles alternate during each half-cycle of the AC waveform. This behavior depends on the polarity of the AC magnetomotive force relative to the permanent magnet bias.

Consequently, the device transitions from a total inductance of $2L_s$ during normal operation to $L_s + L_u$ under fault conditions. Since $L_u \gg L_s$, the effective inductance increases

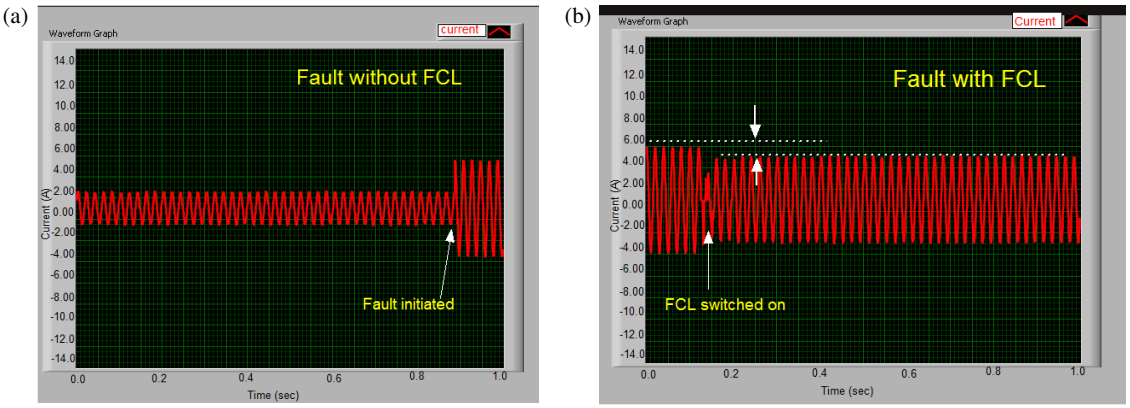

FIGURE 11. (a) Measured current waveform during a fault without the FCL. (b) Current waveform during fault with FCL.

sharply, producing a substantial rise in impedance. This inductance variation suppresses the fault current. The alternating saturation of the two cores, therefore, constitutes the fundamental physical mechanism underlying current suppression in the PM-FCL.

6.7. Experimental Validation Based on a Laboratory Prototype

To validate the analytical model and finite-element results, a laboratory-scale prototype of the proposed PMFCL was developed and tested, shown in Fig. 10. The experiment evaluates the current suppression capability under controlled conditions.

The objective of the prototype study is to demonstrate functional feasibility and confirm the underlying current-limiting mechanism. The setup is not intended to replicate full-scale distribution-level operation but to verify device behaviour at reduced power levels. The prototype design parameters were obtained using the Particle Swarm Optimization (PSO) framework. This approach ensured appropriate trade-offs among peak current suppression, recovery characteristics, and core losses.

6.7.1. Prototype Setup and Instrumentation

A photograph of the experimental setup is shown in Fig. 10. The developed prototype represents a laboratory-scale PMFCL module mounted on a non-magnetic base. The setup includes the magnetic core assembly, excitation winding, and permanent magnet biasing arrangement based on the optimized design parameters obtained through PSO-based modelling. The prototype is connected to a single-phase AC supply through appropriate protection and switching elements.

Current and voltage are measured using calibrated sensors. The acquired signals are processed through a data acquisition unit (NI USB-6009) and transferred to a PC for real-time monitoring and systematic data recording. An oscilloscope (CRO) is used to verify transient waveforms and ensure measurement reliability. Fault conditions are emulated by abruptly changing the load impedance at a predefined time instant. This approach enables controlled and repeatable reproduction of fault scenarios.

6.7.2. Experimental Procedure

Two operating cases were evaluated under identical supply and pre-fault conditions. In the first case, a fault was applied without the PMFCL connected to the circuit. In the second case, the same fault condition was introduced with the PMFCL inserted and activated. This approach enables direct and consistent comparison between the two scenarios.

The fault was initiated at approximately $t = 0.2$ s, and current waveforms were recorded for a total duration of 1 s. The sampling rate was selected to capture both the transient response at fault inception and the subsequent steady-state behaviour with adequate resolution.

The operating parameters correspond to the optimized values obtained from the PSO framework. This ensures that the experimental investigation accurately evaluates the intended performance of the designed PMFCL.

6.7.3. Experimental Results

The measured fault current without the PMFCL is shown in Fig. 11(a). Immediately after fault initiation, the line current rises rapidly to a peak value of approximately 5.5 A, corresponding to about 10.7 A peak-to-peak. This increase occurs because no limiting impedance is present in the circuit.

The measured current waveform with the PMFCL inserted is shown in Fig. 11(b). In this case, the maximum fault current is limited to approximately 3.1 A, corresponding to about 6.2 A peak-to-peak. The reduction occurs immediately after activation of the PMFCL, and the current stabilizes within one fundamental cycle.

Based on the measured waveforms, the experimental reduction in peak fault current is approximately 42%. Although the absolute current levels are lower than FEM predictions due to laboratory scale and supply constraints, the observed reduction ratio and transient behaviour agree well with the analytical model and PSO-optimized design trends.

6.7.4. Discussion and Experimental Scope

The experimental results demonstrate that the proposed PM-FCL introduces additional impedance under fault conditions,

thereby suppressing excessive current rise and stabilizing the system response. The observed behaviour aligns with analytical predictions and finite-element simulations, confirming the physical validity of the PSO-based optimization framework, as shown in Table 9.

TABLE 9. Experimental fault current measurements.

Operating condition	Peak current (A)	Peak-to-peak current (A)
Normal operation	1.8	3.6
Fault without FCL	5.5	10.7
Fault with FCL	3.1	6.2

The present study is limited to short-duration laboratory tests on a scaled prototype. Long-term thermal effects, progressive magnet demagnetization, and manufacturing tolerances were not investigated and remain subjects for future work. Nevertheless, the measurements provide direct experimental evidence of the current suppression mechanism and validate the PSO-guided design methodology at the proof-of-concept level. Future research will focus on prototype scale-up, coupled thermal-magnetic modelling, and extended fault testing under practical operating conditions.

6.8. Validation of Simulation and Experimental Results

Figure 11 presents the measured current waveforms under fault conditions without and with the PMFCL inserted. The prototype results confirm substantial current suppression when the limiter is active. To further assess consistency, the experimental results are compared with corresponding FEM simulations (Table 10). Although absolute current magnitudes differ due to laboratory-scale limitations, the two approaches exhibit the same qualitative behaviour: rapid current rise at fault inception, followed by amplitude suppression and waveform stabilization.

TABLE 10. Comparison of simulated and experimental fault current levels.

Operating condition	FEM simulation peak current	Experimental peak current
Fault without FCL	6.0 kA	5.5 A
Fault with FCL	1.2 kA	3.1 A

The reduced mitigation level observed experimentally is attributed to practical constraints of the prototype, including limited supply voltage, non-ideal switching elements, and simplified construction. Despite these differences, consistent current-limiting trends are observed across analytical modelling, FEM simulations, and laboratory measurements. This agreement provides strong physical evidence of the robustness of the optimized design and the effectiveness of the PSO-based optimization strategy.

Although Table 10 confirms the agreement between FEM simulations and laboratory measurements for the single-phase PMFCL, the results also support extension to multi-phase and higher-voltage systems. The modular optimization framework enables independent phase-level design while preserving electromagnetic performance, current suppression capability, and thermal and magnetic safety margins.

Design constraints, such as maximum temperature $(T_{\max}|T_{safe})$ and demagnetization limits $(H_m|H_{c,safe})$, can be incorporated directly into the optimization process. Additional high-voltage requirements, including insulation coordination, increased air gaps, and mechanical clearances, can be integrated without compromising limiting effectiveness. These results demonstrate that the optimized single-phase PMFCL can serve as a scalable and reliable building block for medium- and high-voltage applications.

7. DISCUSSION OF OPTIMIZATION AND PERFORMANCE

The optimized PMFCL demonstrates improved electrical performance with enhanced material efficiency compared with conventional designs. The permanent magnet bias maintains low inductance during normal operation. The optimized core geometry and winding configuration enable rapid inductive response under fault conditions. Steady-state voltage waveforms remain stable, indicating minimal voltage drop in normal operation. Parametric and surface analyses of the current suppression ratio (CSR) with respect to saturated relative permeability (μ_s) and total winding turns (N) reveal important design trade-offs in Fig. 4. Increasing μ_s enhances the inductive response during faults. However, excessive permeability drives the core into deeper saturation, which reduces incremental performance gains. The optimal design region therefore corresponds to moderate parameter values that provide strong suppression capability without excessive core volume, copper losses, or material cost.

A sensitivity analysis was conducted by varying the weighting coefficients associated with peak fault current, core volume, and steady-state losses in the multi-objective formulation. The optimized solutions remain consistent across a wide range of weighting combinations. This confirms the robustness of the proposed optimization framework and the stability of the obtained design.

7.1. Convergence Characteristics of Optimization Algorithms

The convergence behaviour of the Genetic Algorithm (GA), Particle Swarm Optimization (PSO), and Pattern Search (PS) is shown in Fig. 12. All algorithms were evaluated using the same design variables, parameter bounds, and weighting factors to ensure a fair comparison.

Although GA and PSO exhibit rapid initial reduction in the objective function, their convergence trajectories are oscillatory and require more iterations to achieve stable solutions. In contrast, Pattern Search shows monotonic and stable convergence and achieves a lower final objective value with fewer function evaluations. As summarized in Table 3, Pattern Search requires approximately 15 iterations for convergence, whereas GA and PSO require nearly 40 iterations.

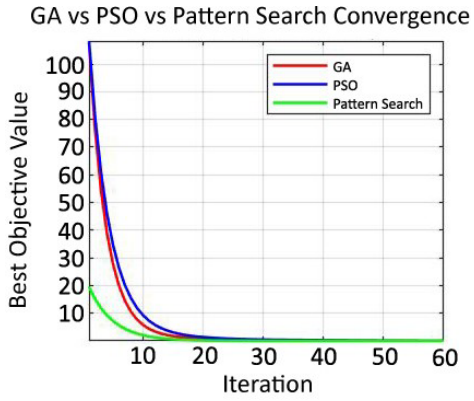

FIGURE 12. Convergence characteristics of GA, PSO, and Pattern Search for the optimized PMFCL.

The derivative-free and deterministic nature of Pattern Search eliminates the need for algorithm-specific tuning of population size or control parameters. This property makes it well-suited for nonlinear and non-smooth optimization problems commonly encountered in PMFCL design. These characteristics enable efficient optimization while balancing fault current reduction, core size, and steady-state losses.

7.1.1. Applicability to Three-Phase and High-voltage Systems

Although the current work is based on a single-phase PMFCL configuration, the proposed optimization framework is modular in nature and easily extendable to three phases. In a three-phase arrangement, it is possible to optimize each phase independently while considering the inter-phase magnetic coupling effects by using additional constraint terms in the objective function. This allows controlling the peak fault current phase-wise, CSR, core losses, and permanent magnet operating margins.

The same saturation-based operating principle and permanent magnetic biasing mechanism can be made using three-phase modular or stacked magnetic structures. For high voltage applications, other design constraints such as insulation coordination, creepage and clearance distances, dielectric strength, and mechanical spacing can be imposed directly onto the optimization framework. The gradient-free property of The Pattern Search algorithm is ideal for use with these nonlinear and multi-constraint design environments.

Thermal limits and demagnetization safety margins of the permanent magnets can also be applied as phase-wise limitations in order to ensure safe operation under severe fault conditions. While the experimental validation of a complete prototype in three-phase or high-voltage is not in the scope of the present study, a workable and scalable path to the deployment of medium and high voltage PMFCL has been developed.

8. CONCLUSION

This paper provides a detailed design and optimization scheme of a permanent magnet biased fault current limiter (PMFCL). The methodology combines a magnetic circuit model based on a power system, finite element validation, and the derivative-free optimization by pattern search. By taking into account the peak fault current, core material consumption, and steady-state losses at the same time, the framework results in an efficient and compact design solution. The electromagnetic analysis confirms that deep saturation is sustained in normal operation to ensure low insertion impedance and partial desaturation in the presence of a fault, causing a rapid increase of inductance to limit the current in the fault effectively. Parametric and surface analyses are further used to understand the trade-offs of permeability and turns of the winding, volume of material, and loss performance. A comparative evaluation of genetic algorithm (GA), particle swarm optimization (PSO), and pattern search shows that, although population-based methods are useful to give fast initial convergence, pattern search gives more stable and reliable convergence for the highly nonlinear and saturation-dominated PMFCL design space. This validates the suitability of the derivative-free optimization approach. A laboratory-scale prototype was made in order to validate the proposed design methodology. Experimental results prove the good fault current suppression and achieve effective qualitative agreement with analytical and finite-element predictions to achieve proof-of-concept validation.

Future work will focus on three-phase implementation, high power and long-duration experimental work, coupled thermal-magnetic modelling, as well as long-term evaluation of thermal aging and permanent magnet stability. The calibration of Steinmetz parameters of loss by using manufacturer data or dedicated measurements will increase predictive accuracy more.

REFERENCES

[1] Dong, Y., J. Zhu, D. Wei, W. Chen, Q. Du, K. Zhang, P. Chen, K. Lu, H. Jiang, S. Wang, J. Liu, T. Guo, and K. Ding, "10 kV AC test verification of the high temperature superconducting fault current limiter with bias magnetic field," *Cryogenics*, Vol. 112, 103195, 2020.

[2] Morandi, A., "Fault current limiter: An enabler for increasing safety and power quality of distribution networks," *IEEE Transactions on Applied Superconductivity*, Vol. 23, No. 6, 57–64, 2013.

[3] Kim, J.-S., S.-H. Lim, J.-C. Kim, and J.-F. Moon, "A study on bus voltage sag considering the impedance of SFCL and fault conditions in power distribution systems," *IEEE Transactions on Applied Superconductivity*, Vol. 23, No. 3, 5601604, Jun. 2013.

[4] Harzig, T. and B. Grainger, "Time-optimal finite control set model predictive control of non-isolated DC-DC converters," *IET Electric Power Applications*, Vol. 18, No. 11, 1626–1637, 2024.

[5] Yuan, J., Y. Sun, W. Zhang, Y. Liu, H. Zhou, and H. Zhong, "A novel hybrid magnetic material based on three-phase saturated core fault current limiter," *AIP Advances*, Vol. 14, No. 2, 025301, Feb. 2024.

[6] Das, S., T. Santra, A. B. Choudhury, D. Roy, and S. Yamada, "Transient modeling and performance analysis of a passive magnetic fault current limiter considering JA hysteresis model," *Electric Power Components and Systems*, Vol. 47, No. 4–5, 396–405, 2019.

[7] Eladawy, M. and I. A. Metwally, "Compact designs of permanent-magnet biased fault current limiters," *IET Electric Power Applications*, Vol. 14, No. 3, 471–479, 2020.

[8] Das, S., A. B. Choudhury, T. Santra, and T. S. Daphadar, "Finite element analysis of a passive magnetic fault current limiter using adaptive meshing," *IET Conference Proceedings*, Vol. 2020, No. 8, 64–68, 2020.

[9] Santra, T., A. K. Chkraborty, D. Roy, and A. B. Choudhury, "Analysis of passive magnetic fault current limiter using wavelet transform," in *2009 International Conference on Power Systems*, 1–6, Kharagpur, India, 2009.

[10] Das, S., A. B. Choudhury, T. Santra, and S. Pramanik, "Performance analysis of a passive magnetic fault current limiter under the influence of shorting ring," in *2021 International Conference on Control, Automation, Power and Signal Processing (CAPS)*, 1–5, Jabalpur, India, 2021.

[11] Das, S., A. B. Choudhury, T. Santra, and C. K. Chanda, "Analysis of permanent magnet fault current limiter considering faults occurring at various position of a rectifier circuit load," *Microsystem Technologies*, Vol. 30, No. 10, 1249–1258, 2024.

[12] Eladawy, M. and I. Metwally, "Stacked delta design of three-phase permanent-magnet fault current limiters," *The Journal of Engineering Research*, Vol. 18, No. 1, 26–35, 2021.

[13] Das, S., T. Santra, A. B. Choudhury, D. Roy, and S. Yamada, "Estimating and minimizing the eddy current loss in a permanent magnetic fault current limiter," *International Journal of Emerging Electric Power Systems*, Vol. 25, No. 1, 109–117, 2024.

[14] Das, S., T. Santra, and A. B. Choudhury, "Power quality assessment of the distribution system containing passive magnetic fault current limiter under normal and fault conditions," *Electric Power Systems Research*, Vol. 254, 112698, 2026.

[15] Wei, L., B. Chen, J. Yuan, C. Tian, Y. Zhong, X. Li, Y. Gao, and K. Muramatsu, "Performance and optimization study of a novel compact permanent-magnet-biased fault current limiter," *IEEE Transactions on Magnetics*, Vol. 53, No. 11, 1–4, 2017.

[16] Baba, K., K. Noro, Y. Kozuka, T. Kumasaka, M. Shinozaki, M. Kawasaki, and T. Otsuka, "Formation of few-electron triple quantum dots in ZnO heterostructures," *Scientific Reports*, Vol. 15, No. 1, 36612, 2025.

[17] Wu, J., J. Chen, J. Liu, J. Yuan, Y. Gan, H. Zhou, and B. Yuan, "The performance investigation and material optimization of three-phase saturated core fault current limiter," *IEEE Transactions on Magnetics*, Vol. 61, No. 9, 1–7, Art No. 8400807, Sept. 2025.

[18] Usama, M., H. Mokhlis, N. N. Mansor, M. Moghavvemi, M. N. Akhtar, A. A. Bajwa, and L. J. Awalin, "A multi-objective optimization of FCL and DOCR settings to mitigate distributed generations impacts on distribution networks," *International Journal of Electrical Power & Energy Systems*, Vol. 147, 108827, 2023.

[19] Akin, F. and O. Arikan, "Hybrid meta-heuristic and non-dominated sorting based optimization for DG and FCL placement considering long-term economic profitability," *Electric Power Systems Research*, Vol. 253, 112487, 2026.

[20] Sarangi, R. R., P. K. Ray, S. Swain, M. Sahoo, and A. Mohanty, "Performance optimization of FCL in DC microgrid using meta heuristic techniques," in *2024 IEEE International Conference on Power Electronics, Drives and Energy Systems (PEDES)*, 1–5, Mangalore, India, 2024.

[21] Dey, N. and T. Santra, "Application of PSO for optimizing gain parameters of a controller in real system," in *Michael Faraday IET International Summit 2015 (MFIIS 2015)*, Kolkata, India, 2015.